Journal of Water Process Engineering 33 (2020) 101005

Contents lists available at ScienceDirect

Journal of Water Process Engineering

journal homepage: www.elsevier.com/locate/jwpe

Tailoring the surface properties of carbon nitride incorporated thin film nanocomposite membrane for forward osmosis desalination

A. Abdul Aziz[a,b], K.C. Wong[a,b], P.S. Goh[a,b,*], A.F. Ismail[a,b], I. Wan Azelee[a,b]

[a] Advanced Membrane Technology Research Centre (AMTEC), Universiti Teknologi Malaysia, 81310, Skudai, Johor, Malaysia
[b] School of Chemical and Energy Engineering, Faculty of Engineering, Universiti Teknologi Malaysia, 81310, Skudai, Johor, Malaysia

ARTICLE INFO

Keywords:
Carbon nitride
Reverse osmosis
Forward osmosis
Thin film nanocomposite

ABSTRACT

Thin film nanocomposite (TFN) membranes incorporated with carbon nitride (CN) or protonated CN (pCN) were fabricated for forward osmosis (FO) desalination. The CN and pCN were incorporated within the polyamide (PA) layer which was supported by pCN incorporated polysulfone (PSf) substrate to form the TFN membrane. It was found that the presence of pCN in the substrate has favourably altered the intrinsic properties and affected the formation of PA layer. The physico-chemical characterizations indicated that the presence of both CN and pCN enhanced the surface hydrophilicity but reduced the surface negativity of the PA layer. These features have resulted in the improved water transport and salt rejective ability. As a result, CN-pCN-TFN membranes exhibited improved water permeability by about 70% (0.67 L/m^2 h bar) compared to TFC membrane while maintaining salt rejection of 94.5%. CN-pCN-TFN also exhibited better anti-fouling property compared to TFC in which the flux decline was only half of that of TFC membrane during the 9 -h antifouling test. This work demonstrates the feasibility of using functional CN and pCN to independently tailor the substrate and PA layer properties of the TFN membrane, hence improving the desalination performances of the membrane.

1. Introduction

Human population in the world has reached 7 billion in 2015 and the number keeps increasing with nearly 250 thousand added daily. The population is expected to reach 9.7 billion by 2050 [1]. The major issue that accompanies the exponentially growth population is the shortage of fresh water supply. As reported by United Nations World Water Development in 2015, 780 million people did not have access to safe drinking water and this number is expected to raise in the coming years [2,3]. Numerous alternatives have been considered to address this global challenge. Desalination is one of the most promising methods to recover fresh water supply considering the amount of seawater that exist and the limited resources of fresh water available [4–6]. Forward osmosis (FO) has attracted attention in the desalination community due to its desirable features for sustainable desalination process [7]. By carefully selecting an appropriate draw solution and a regeneration approach that requires low energy consumption, FO holds great potential as an alternative to commercially used RO [8]. Currently, the main obstacle that limits the performance of FO is the internal concentration polarization (ICP) [9]. ICP is a phenomenon resulted from the accumulation of solutes inside of the pore of the membrane which in turn changes the effective osmotic pressure that act as driving force [10].

Thin film composite (TFC) membrane has been widely used for FO desalination owing to its high salt rejection and water flux. Typically, TFC comprises of a polyamide (PA) layer which is fabricated on top of a polymeric substrate through an interfacial polymerization (IP) process [4,11]. Over the last decade, the advancement made in nanoscience and materials has provided unprecedented means to address the underlying issues related to the limitations of TFC membranes. The incorporation of various functional nanomaterials in thin film nanocomposite (TFN) membranes has rendered some attractive features to strengthen the membrane properties such as anti-fouling, membrane morphology and most importantly the performance. The first attempt of making such effort can be dated back to 2007 where nanoparticles such as zeolite and carbon nanotubes (CNT) were introduced to improve the mechanical, chemical, thermal, and separation behaviour of the membrane [12]. Recently, graphene-based nanomaterials and metal oxide framework (MOF) have been the subjects of focus as they are known to provide high permeability and selectivity to the resultant TFN, hence, greatly reduce the energy consumption in filtration while maintaining high recovery [13]. The incorporation of nanomaterials with super hydrophilic properties and negative surface charges is able to improve the anti-fouling performance and permeability without sacrificing the

* Corresponding author at: Advanced Membrane Technology Research Centre (AMTEC), Universiti Teknologi Malaysia, 81310, Skudai, Johor, Malaysia.
E-mail address: peisean@petroleum.utm.my (P.S. Goh).

https://doi.org/10.1016/j.jwpe.2019.101005
Received 19 July 2019; Received in revised form 30 September 2019; Accepted 14 October 2019
Available online 05 November 2019

superior salt rejection [14]. As reported by Pan et al. [15], blending of imogolite nanotubes into the PSf substrates has significantly improved the hydrophilicity, water flux, porosity and roughness of the membrane surface. Ghanbari et al. who reported the blending of HNT within PSf substrates have also observed enhancement in the water permeability due to increase in hydrophilicity and porosity of the resultant TFN compared to the TFC membrane [10]. Additionally, Emadzadeh et al. reported that the embedment of titanate nanotubes (NH_2-TNTs) in PA layer has improved the TFN salt rejection by 2% and water flux by almost two folds compared to that of TFC [16].

Recently, graphitic carbon nitride (CN) has attracted attention in various applications [17]. CN forms graphene-like nanosheets structure and has a diamond-like mechanical properties [18,19]. CN can be used as metal-free photocatalyst for the degradation of organic pollutions owing to its special optical feature, high thermal stability and chemical stability [20]. According to Wang et al., CN has the potential to enhance wettability of composite substrate through the interaction of hydrogen bonding of water molecules with the nitrogen atoms of CN [21]. Surface modification of nanomaterials is a common strategy to further enhance the functionality or to improve the dispersibility of the nanomaterials when incorporated into polymeric matrix. One of the easiest ways to introduce functional groups to the surface of nanomaterials is through acid modification. Oxidation of the nanomaterials by acid treatment improves the dispersion of the nanomaterials through the generation of hydroxyl and carboxyl functional groups on the nanomaterials structure [22]. Wan Azelee et al. [4] improved the dispersion of multiwalled carbon nanotube and titania nanotube (MWCNT-TNT) hybrid in TMC solution by treating the nanomaterials with sulphuric acid. The embedment of this acid treated hybrid into the PA layer has rendered negative charges and allowed better interaction between the water molecule and the selective layer to produce a highly permeable TFN without compromising the selectivity. In this study, CN was treated with acid to modify the surface charges and functionalities of the nanomaterials. This protonated CN (pCN) was then dispersed into PSf dope solution to fabricate nanocomposite substrate. Additionally, TFNs containing CN or pCN within the selective layer have also been fabricated. The resultant membranes were subjected to various characterizations to investigate the effects of CN and pCN towards the physicochemical properties of the TFN membranes. Finally, the desalination performance was evaluated in terms of the flux and selectivity in RO and FO system. This work represents the first attempt of using CN and pCN to fabricate TFN membrane hence it may provide new insights into the potentials of these nanomaterials in enhancing the performance of TFN for desalination.

2. Experimental

2.1. Materials

Polysulfone Udels P-3500 LCD MB3 polymer, supplied in a form of pellets by Solvay, was used to prepare neat PSf supports. Polyvinylpyrrolidone (PVP, K29-32) and 1-methyl-2-pyrrolidinone (NMP,99.5%) obtained from Acros Organic were used as pore forming agent and solvent, respectively, to develop PSf supports. m-Phenylenediamine (MPD,99%) and 1,3,5-benzenetricarbonyl trichloride (TMC,98%) from Acros Organic were used to prepare TFC membranes (i.e., using PSf as supports). Sodium chloride (NaCl, 99.5%) provided by RCL Labscan and n-hexane (C_6H_6, 49%) were supplied by Merck, while hydrochloric acid (HCl, 65 wt%) was obtained from Merck. Melamine was supplied by Sigma-Aldrich.

2.2. Synthesis of carbon nitride and acid treatment

Melamine precursors were used to synthesize CN through a thermal polycondensation method [23]. In a typical procedure, 15 g of melamine powder was filled into an alumina crucible with lid. Next, the crucible was heated to 550 °C in air condition using Carbolite muffle furnace with a heating rate of 5 °C/min. The furnace temperature was maintained at 550 °C for 2 h before the heating element was turned off to allow the furnace to cool naturally. After the setup was cooled to room temperature, the resulted yellow product was collected and ground into a powder with a ceramic mortar for a further use. For the synthesis of pCN, 10 mL of 5 M hydrochloric acid was mixed with each gram of CN used. The suspension was then stirred overnight, followed by filtration and washing with deionised water to neutralize the product. Lastly, the pale-yellow powder was ground and dried overnight at 100 °C under vacuum condition.

2.3. Preparation of polysulfone (PSf) support membrane

Phase inversion technique was used to fabricate PSf substrates [24]. The dope solution to produce neat PSf substrates was prepared by dissolving 17.5 wt% PSf and 0.5 wt% PVP in NMP. The dope solution was stirred for 24 h to ensure proper dissolution of PSf pellets and homogeneous dispersion of pCN. After that, the dope solution was degassed via sonication in a room temperature for 1 to 2 h. The degassed dope solution was casted onto a clean glass plate using a glass rod, then, immediately immersed into a coagulation bath containing deionised (DI) water. After 2 min, the solidified PSf sheet was peeled from the glass plate, transferred into a second DI water bath and kept overnight to ensure that remnant solvent within the PSf substrate was removed. For the preparation of pCN incorporated PSf substrate (pCN-PSf), the same procedure for preparing neat PSf was used, except 0.5 wt% of pCN was added into the dope solution.

2.4. Preparation of thin film composite and thin film nanocomposite membranes

PA active layer was formed on top of the PSf substrate via IP method using 2 w/v% of MPD in deionised water and 0.1 w/v% TMC in n-hexane. First, the substrate membrane was fixed in-between a glass plate and a rubber frame. Then, the MPD solution was poured into the setup to saturate the exposed side of PSf with the diamine monomer. After 1 min, excess MPD solution was drained off and the leftover droplets were remove using a rubber roller. Next, TMC solution was dripped onto the MPD saturated surface to initiate the IP process. After 50 s, excess TMC solution was poured out and the resulted TFC was left to dry in ambient temperature for 1 min before thermally treated in oven at 60 °C for 5 min. Lastly, the membrane was stored in DI water for 24 h before further use.

For the fabrication of TFN membrane, 0.05 w/v% of pCN or CN was dispersed into the TMC solution. The mixture was then sonicated for 1 h prior to IP to avoid agglomeration of the nanoparticles. The denotations of the TFN membranes prepared in this study are tabulated in Table 1.

2.5. Characterization of nanomaterials and membranes

The morphology of CN and pCN was examined using transmission electron microscopy (TEM, HT 770, Hitachi, Japan). For this purpose, small amount of the powdered sample was dispersed in water via 1 h

Table 1
Denotation use to represent the membranes.

Substrate membrane	PA layer	Denotation
17.5 wt% PSf + 0.5 wt% PVP	2 w/v% MPD + 0.1 w/v% TMC	TFC
17.5 wt% PSf + 0.5 wt% PVP + 0.5 wt% pCN	2 w/v% MPD + 0.1 w/v% TMC	pCN-TFN
17.5 wt% PSf + 0.5 wt% PVP + 0.5 wt% pCN	2 w/v% MPD + 0.1 w/v% TMC + 0.05 w/v% pCN	pCN-pCN-TFN
17.5 wt% PSf + 0.5 wt% PVP + 0.5 wt% pCN	2 w/v% MPD + 0.1 w/v% TMC + 0.05 w/v% CN	CN-pCN-TFN

sonication. After standing for 10 min, the supernatant of the suspension solution was drawn out using a clean pipette then dropped onto a copper grid to deposit the nanomaterials on the grid. The loaded copper grid was dried in oven at 60 °C for 10 min before analysis. X-ray diffraction spectroscopy (XRD, Cu K_α radiation, $\lambda = 0.154$ nm, D/max-rB 12 kW Rigaku) was used to examine the crystallinity of the synthesized nanomaterials. The fine sample powder was packed onto a sample holder before loaded into the XRD spectrometer. The scanning was carried out at 2θ between 4° and 70°. The functional groups of CN and pCN were identified via Fourier transmission infrared spectroscopy (FTIR, Thermo Nicolet Avatar 360). The sample was mixed with KBr powder via grinding for 2 min. Then the homogenized powder was compressed into a thin pellet using a stainless-steel die. The pellet was loaded into the sample holder and the FTIR scanning was carried out at wavenumber between 400 cm^{-1} and 4000 cm^{-1}. To determine the surface charge, surface zeta potential (Malvern Zetasizer Nano ZS) was used. The sample were prepared by using deionized water as a medium (pH neutral, at room temperature) and with dispersant dielectric constant of 78.5. For membrane sample, average pore diameter and porosity of the PSf and pCN-PSf substrate were determined by using mercury porosimeter (MicroActive AutoPore V 9600, Micromeritics Instrument Corp.) FTIR was conducted in attenuated total reflectance mode (ATR-FTIR) by switching the pellet holder of the spectrometer into ATR accessories. Membrane sample was cut into strips then clamped on the ATR probe and scanned at wavenumber between 600 cm^{-1} and 4000 cm^{-1}. Other than that, the morphological structure of the membrane was investigated using field emission scanning electronic microscope (FESEM, SU8020, Hitachi). Prior to scanning, membrane sample was cut into a 10 mm × 2 mm strip, taped onto a metallic stub using carbon tape then sputter coated with gold. In the case of cross-sectional scan, membrane sample was snapped after frozen in liquid nitrogen for 1 min to avoid structural change in membrane resulted by cutting tools. Other than that, surface roughness of membranes (R_a) was measured using atomic force microscope (AFM, SII Nano Technology SPA 300 HV). 10 mm × 10 mm of pre-cut membrane sample was adhered onto a flat glass slide before loaded onto the AFM probing stage for characterization. Membrane surface charge was determined by zeta potential test (Malvern Zetasizer Nano ZS). Lastly, the wettability of the membrane was examined via sessile drop technique using contact angle goniometer (OCA 15 Pro, Dataphysics). All membrane samples were dried under ambient condition for 24 h prior sample preparation for characterization.

2.6. Evaluation of membrane performances

Dead-end filtration system was used to measure RO performance that was made of stainless steel 316 (Model HP4750 Stirred Cell, Sterlitech Corp., Kent, WA). The membrane active surface area (A_m) was 14.6 cm^2 (2.26 in^2). Firstly, the membrane was stabilized at 16 bar for 30 min with RO water to compact the structure of the membrane. Then, the feed pressure (ΔP in bar) was adjusted to 15 bar and the rate of water permeated through the membrane (Q in L h^{-1}) was measured. Based on the results, the water permeability was calculated using the equation below:

$$\text{water permeability}\,(\text{L}\,m^{-2}\,h^{-1}\,bar^{-1}\text{ or LMH bar}^{-1}) = \frac{Q}{A_m\,\Delta P}$$

Next, the content of the filtration cell was replaced with NaCl solution (2000 ppm) for further testing. The conductivity of the permeated solution was measured using Jenway conductivity meter (Model 4520). Since conductivity is linearly correlated to the concentration of the salt solution, the salt rejection was determined based the equation below:

$$\text{salt rejection}\,(\%) = \left(1 - \frac{C_p}{C_f}\right) \times 100$$

where C_p is the conductivity of permeate solution and C_f is the conductivity of feed solution.

Other than that, filtration performance of the membrane in two FO modes i.e. active layer facing feed solution (AL-FS) and active layer facing draw solution (AL-DS) were also tested. For this experiment, PTFE cell (CF016P-FO cell) with A_m of 20.6 cm^2 (3.2 $inch^2$) which was supplied by Sterlitech Corp was used. The draw solution consisted of 2 mol L^{-1} NaCl while distilled water was used as the feed solution, respectively. Prior to variables measurement, membrane sample was first stabilized for 30 min. After that, the changes in the weight of draw solution and the conductivity of feed solution were monitored and recorded for every 30 min test using digital weighing balance (Model GX-12 K, A & D Company Limited, Toshima-ku, Tokyo) and portable conductivity meter (Model Pro30, YSI, Yellow Springs, OH), respectively. 3–4 consistent readings were taken to compute the average water flux (J_v in LMH) and reverse solute flux (J_s in gMH). The following equations were used for the calculation of J_v and J_s, respectively.

$$J_v = \frac{\Delta m}{\Delta t\, A_m\, \rho_{H_2O}}$$

$$J_s = \frac{\Delta(C_t\, V_t)}{\Delta t\, A_m}$$

Where ρ_{H_2O} is the density (in g L^{-1}) of water while Δt is the duration (in h) of water permeation. C_t is the concentration (in g L^{-1}) of the salt solution at the end of permeation time and V_t is the volume (in L) of permeated water at the end of permeation time. The antifouling property of the best TFN membrane was evaluated in AL-FS mode using sodium alginate and bovine serum albumin (BSA) as model foulants. Solution of 500 ppm sodium alginate or BSA was used as the feed solution during anti-fouling test and the changes in water permeability was recorded for a period of 9 h.

3. Results and discussion

3.1. Characterizations of CN and pCN

Morphological structure of CN and pCN was characterized using TEM and illustrated in Fig. 1a and b. As shown, the structure of CN and pCN resembles that of graphene sheets, which is similar to that of reported by Niu et al. [18]. Upon the acid modification, the stacking of pCN nanosheets has been reduced as compared to CN. This can be related to the Derjaguin, Landau, Verwey and Overbeek (DLVO) theory which mentions about the existence of electrical forces between a double layer and also van der Waals forces to stabilize a colloidal system [25]. This was also reported by Wan Azelee et al. [4], where the acid treated MWCNT and TNT showed less entanglement within its molecular structure because of the high repulsive forces that presence on its surfaces. Similar observations have also been made by Mudunkotuwa et al. who treated TiO_2 using citric acid [26].

Fig. 1c presents the XRD patterns of CN and pCN. There are two characteristic peaks for the formation of these nanomaterials, i.e. the peak at approximately 12.48° that corresponds to the in-planar repeated tri-s-triazine unit and the peak around 28° that represents the interlayer stacking distance (d spacing) between subsequent CN layers [21]. After the protonation process, the higher diffraction angle was shifted from 28° (d = 0.318 nm) to 27.42° (d = 0.325 nm), indicating the increasing of d spacing of the planar graphitic interlayer structure [27–29]. This happened due to the existence of the positively charge hydrogen in the structure which has extended the distance between the CN nanosheets layers.

The ATR-FTIR spectra of CN and pCN are shown in Fig. 1d. The peak exists around 802 cm^{-1} is corresponded to the s-triazine ring system [30]. The multiple bands or peaks found between 1200 cm^{-1} and 1600 cm^{-1} are related to the characteristic of C–N heterocycle stretches of C–N(-C)-C and C–NH-C units [31]. The broad peaks occurred

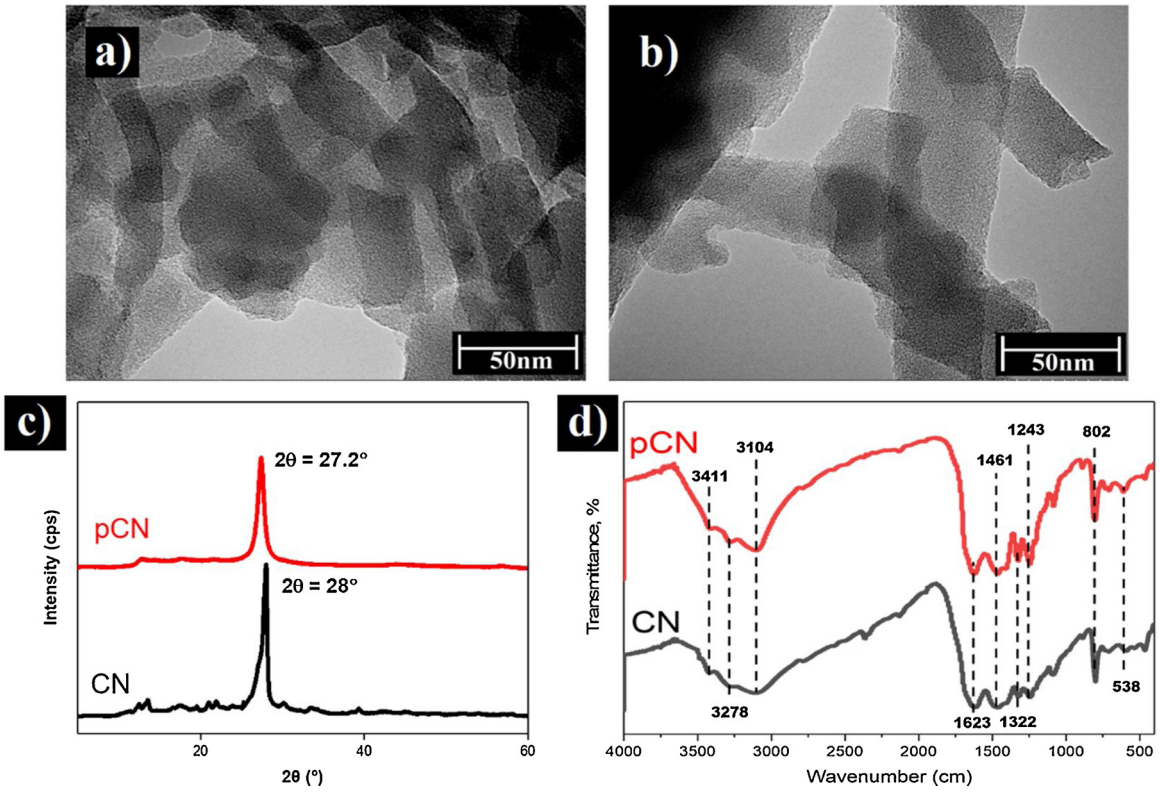

Fig. 1. TEM image of a) CN and, b) pCN, c) XRD of CN and pCN, d) FTIR spectra of CN and pCN.

between 3000 cm^{-1} and 3600 cm^{-1} are due to the N—H stretching. Sharper peaks are observed in pCN due to the higher packing of hydrogen bond [18]. The comparison of the spectra suggested that the basic chemical chains of CN were well maintained after the protonation [32].

The schematic diagram of the formation of CN and pCN is shown in Fig. 2. During the synthesis of CN, melamine precursor was condensed to form CN. Through condensation method, melamine polymer structure rearranged into carbon nitride at 520 °C and formed a diamond-like and graphene-like structure [33]. During the acid treatment, the chemical structure and charges of CN were modified by absorbing positively charged hydrogen from HCl. According to Ong et al. [34], CN surface charge could be easily overturned by treating with acid such as HCl. The positive charges have in turn increased the repulsive force between the molecular structure. The surface charge of CN and pCN was evaluated by measuring the zeta potential. It was found that CN

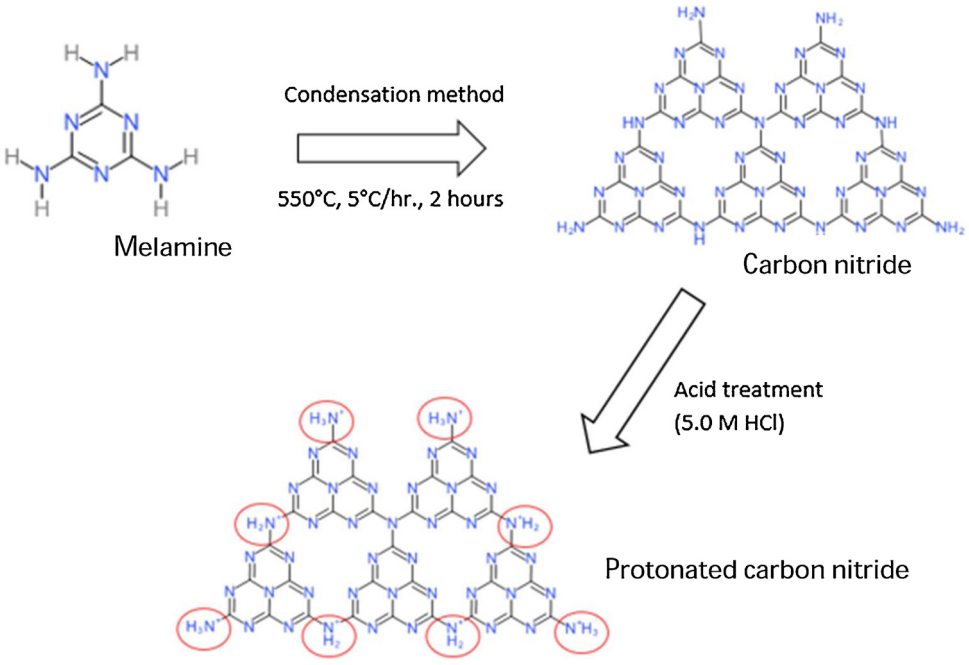

Fig. 2. The schematic diagram that shows the formation of CN and pCN.

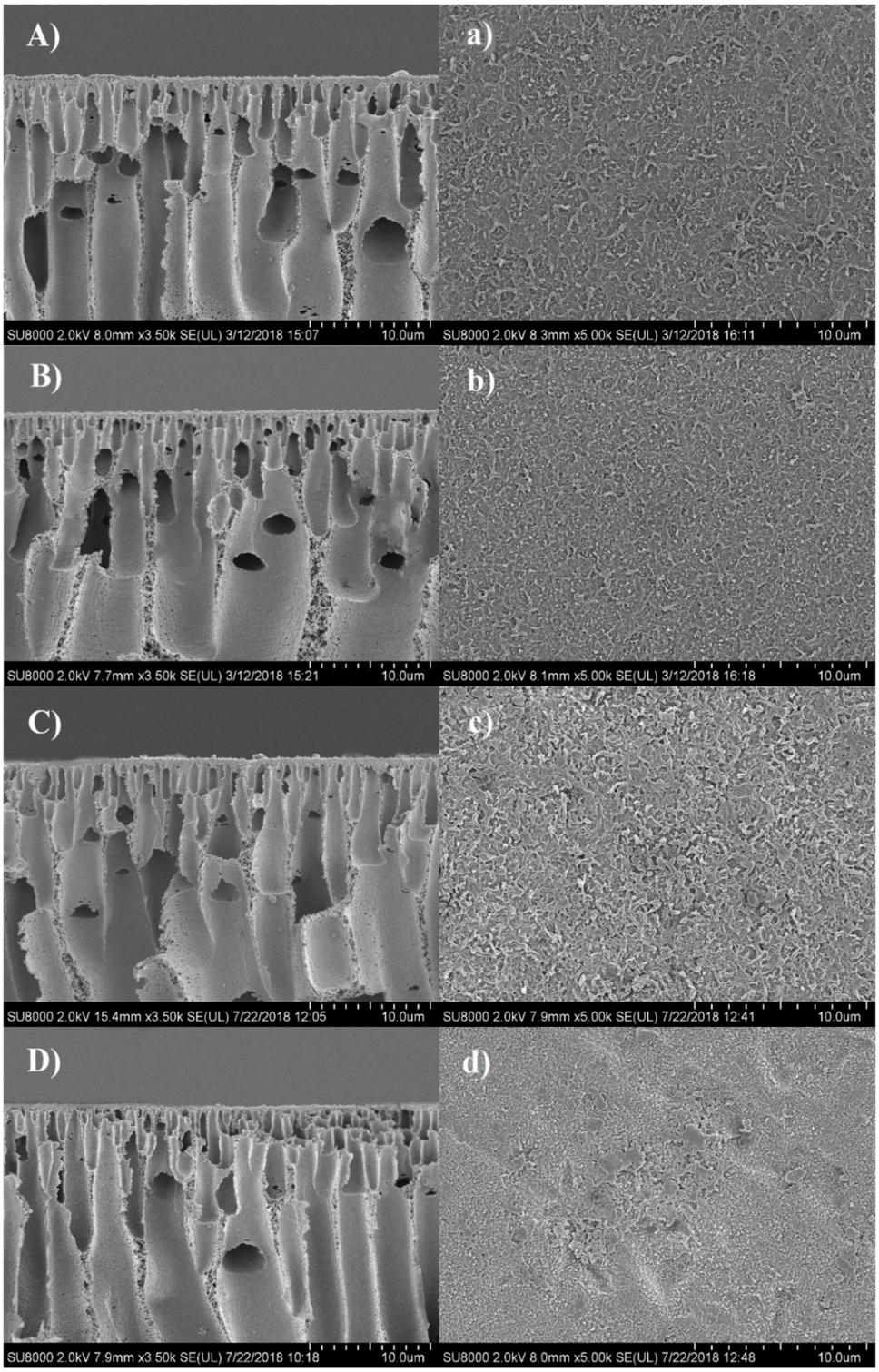

Fig. 3. Cross section (a–d) and surface(a–d) FESEM image of TFC, pCN-TFN, pCN-pCN-TFN and CN-pCN-TFN, respectively.

showed negative charge (-34.6 mV) and increased to positive charge (8.3 mV) after the acid treatment. The change in the surface charges has further verified the successful protonation of CN.

3.2. Characterization of membrane

The surface and cross-sectional morphology of the membranes are illustrated in Fig. 3. The typical cross-sectional images of TFC and TFN membrane that consist of PA thin film layer and PSf substrate are shown in Fig. 3 (a–d). From the cross-sectional images, finger-like structure can be observed across the membrane [14,35,36]. The average pore diameter and total porosity of PSf substrate were 146.85 nm and 74.7% respectively. After incorporating pCN, average pore diameter reduced to 99.27 nm and its total porosity also decreased to 48.9%. The increase in the viscosity of casting solution upon the addition of pCN has lead to the delayed demixing of solvent and non-solvent hence denser structures of substrate were formed. Due to the low loading of both CN and pCN in the substrate and PA layer, the nanoparticles cannot be visibly

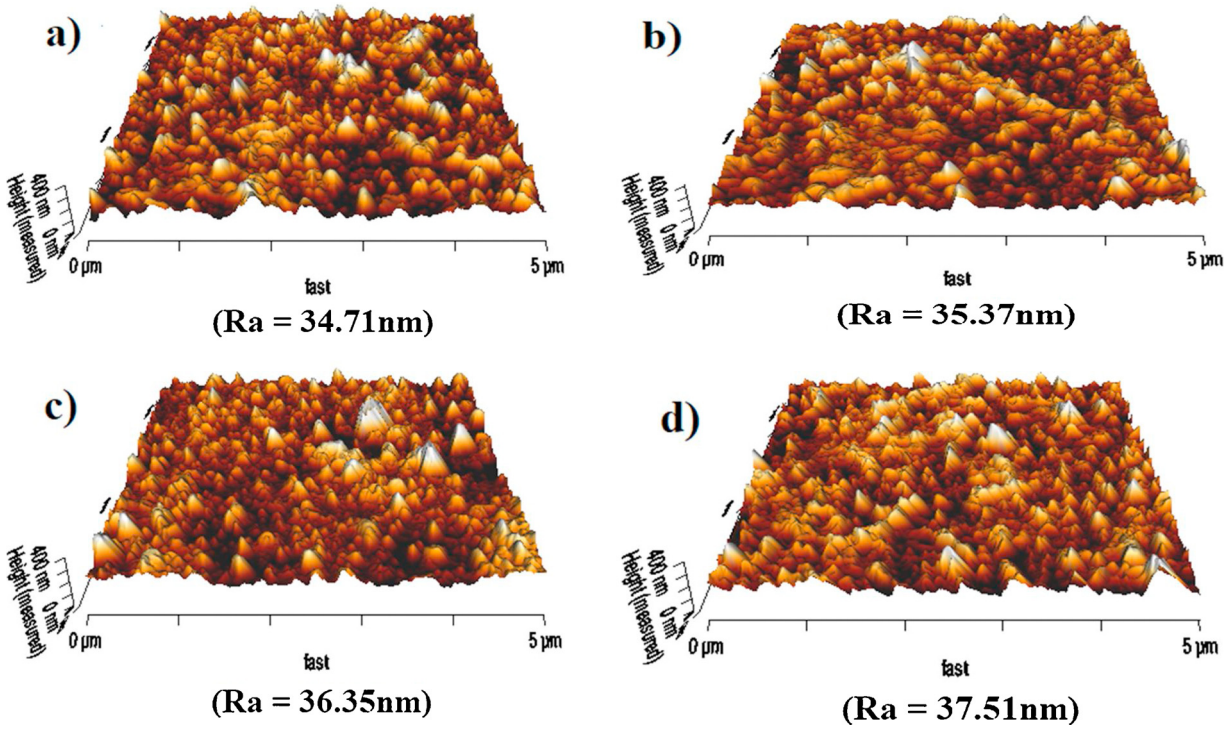

Fig. 4. Three-dimensional AFM images of (a) TFC; (b) pCN-TFN (c) pCN-pCN-TFN; and (d) CN-pCN-TFN.

observed from the membrane cross section. Fig. 3a and b show the surface image of TFC and pCN-TFN. Meanwhile, Fig. 3c and d show the surface images of pCN-pCN-TFN and CN-pCN-TFN where the PA layer has been embedded with CN and pCN, respectively. The difference of Fig. 3c and d compared to that of Fig. 3a and b implied that the incorporation of CN and pCN has influenced the surface morphology of the membranes. Fig. 3a–c show that the ridge and valley structure combined with leaf-like structure were observed and showing the typical PA layer structure of the membrane [37]. Nevertheless, the change in the structure of PA layer in Fig. 3d was probably due to the dispersion of CN. It has been reported that, the incorporation of nanoparticles within the PA may reduce the contact of MPD and TMC during IP process hence affecting the selectivity of the PA layer [38].

Three-dimensional AFM images of the membranes and their average surface roughness (Ra) are shown in Fig. 4. Surface roughness of the TFN membrane was influenced by PA layer that showed a ridge-and-valley structure which caused by the polymerized film of amine and acyl chloride monomers [4,39]. Comparison between Fig. 4a (TFC) and Fig. 4b (pCN-TFN) shows that the surface roughness has slightly increased from 34.71 nm to 35.37 nm due to the presence of pCN in the substrates. Similar observation has also been made by Lai et al. who embedded GO within the substrate [40]. This value increased to 36.35 nm and 37.51 nm for pCN-pCN-TFN and CN-pCN-TFN, respectively.

ATR-FTIR analysis was performed to confirm the existence of the functional group and molecular bonding. As demonstrated in Fig. 5, the peaks at wavenumber 1503 cm^{-1} (CH_3—C—CH_3 stretching), 1409 cm^{-1} (C=C aromatic ring stretching), 1322 cm^{-1} (C—N aromatic amine stretching), 1294 cm^{-1} (asymmetric O=S=O stretching), 1240 cm^{-1} (asymmetric C—O—C stretching) and 1150 cm^{-1} (symmetric O=S=O stretching) were the typical peaks for PSf [28]. While the formation of PA layer was evidenced through the peaks at 1610 cm^{-1} (aromatic ring breathing, C_6H_6), 1585 cm^{-1} (C—N stretching), and 1552 cm^{-1} (NH bending) [41]. The peak observed around 1660 cm^{-1} due to the primary amide stretching can be attributed to the presence of PVP which was used as pore former [42].

Table 2 tabulates the contact angle and surface zeta potential of the membranes. It was noted that the water contact angles of CN-pCN-TFN (56.16 ± 2.92°) and pCN-pCN-TFN (59.74 ± 3.19°) were drastically lower than that of TFC (88.92 ± 3.24°) and pCN-TFN (76.11 ± 3.33°). This implies that the PA layer containing CN or pCN was more easily wetted by water compared neat PA. The elevated affinity of the surfaces of CN-pCN-TFN and pCN-pCN-TFN toward water was attributed to the presence of hydrophilic CN and pCN in the PA layer. In term of zeta potential analysis, the surface of TFC was the most negatively charged (-47.3 mV) among the fabricated membranes in this study. This observation is in agreement with past studies which reported that the surface charge of TFC was in-between −40 mV and −60 mV [43–45]. Upon addition of pCN into the substrate layer, the surface of pCN-TFN was 11.6 mV less negative than TFC. It is believed that the positive charge carried by the pCN within the substrate has contributed to the large drop in negativity of the overall membrane surface charge. This effect was also observed in pCN-PSf where the addition of 0.5 wt% pCN resulted in increased surface zeta potential that of neat PSf from -20.4 mV to -9.06 mV.

On the other hand, due to the small amount of nanofillers incorporated into the PA layer, difference in the surface charges between pCN-TFN (-35.7 mV) and pCN-pCN-TFN (-32.2 mV) was relatively insignificant. Yet, in the case of CN-pCN-TFN, the membrane higher surface change (-28.2 mV) compared to pCN-pCN-TFN was unexpected. Theoretically, the incorporation of negatively charged CN should have resulted to slightly more negatively charged surface of the CN-pCN-TFN compared to pCN-pCN-TFN and pCN-TFN. It is postulated that this deviation could be associated to the structure of the PA layer which was less dense compared to that of pCN-pCN-TFN and pCN-TFN, hence, having lower PA content. Since the negatively charge PA is the primary contributor to the overall surface charge of the membrane, lower PA content would lead to slightly higher zeta potential. This assumption is in line with the data of RO test where the higher water flux but lower salt rejection of CN-pCN-TFN compared to other TFNs could indicate thinner or less dense PA selective layer. According to Margarida et al. [46], negative ions such as chloride ions in the aqueous solution are repelled by the membrane surface that possessed the same charge. Thus, membrane with negatively charged surface is desired to hamper

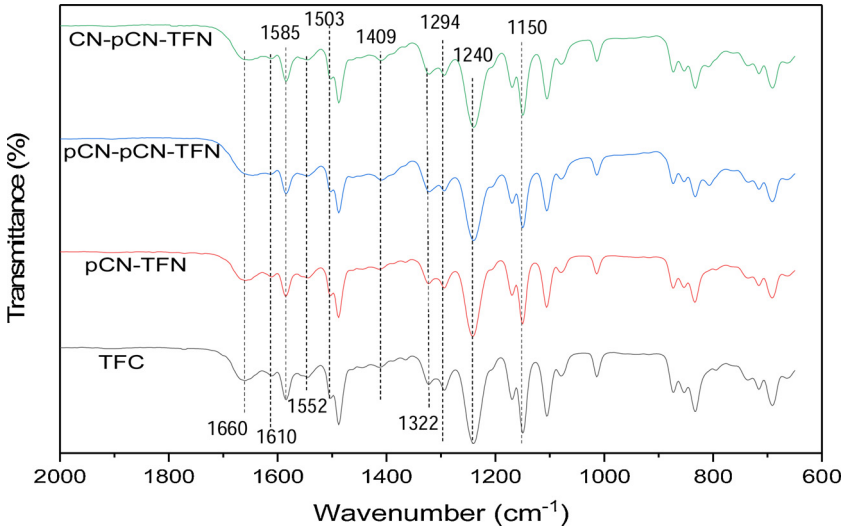

Fig. 5. ATR-FTIR spectra for TFC and TFN membrane.

Table 2
Contact angle and surface charge of TFC and TFN membrane.

Membrane types	Contact angle (°)	Surface zeta potential (mV)
PSf	–	−20.4 ± 2.0
pCN-PSf	–	−9.06 ± 2.6
TFC	88.92 ± 3.24	−47.3 ± 7.1
pCN-TFN	76.11 ± 3.33	−35.7 ± 12.3
pCN-pCN-TFN	59.74 ± 3.19	−32.2 ± 15.6
CN-pCN-TFN	56.16 ± 2.92	−28.2 ± 6.1

the permeation of chloride ions across the membrane.

3.3. Evaluation of desalination performances

Fig. 6 shows the performance of the TFC and TFN membranes in terms of water permeability and salt rejection using RO systems. CN-pCN-TFN membrane exhibited greatly improved water flux when compared to TFC, pCN-TFN and pCN-pCN-TFN membrane. As mentioned earlier, the incorporation of hydrophilic nanoparticles in the substrate and/or PA layer increased the pure water flux. Denser PA layer was formed due to the presence of pCN in the substrate. CN-pCN-TFN membranes exhibited improved water permeability by about 70% (0.67 L/m^2 h bar) compared to TFC membrane. This improvement was influenced by several factors including surface hydrophilicity, surface charge and surface density. These factors were explained in detail in the following parts.

Fig. 7 shows the FO performances of the membrane prepared. Fig. 7A shows the water flux for all membrane prepared in this study. CN-pCN-TFN exhibited the best performance in both AL-FS and AL-DS modes with a result of 6.20 LMH and 9.23 LMH, respectively, Followed by pCN-pCN-TFN with 3.69 LMH and 9.02 LMH, respectively. On the other hand, TFC membrane only showed water flux of 0.78 LMH for in AL-FS mode. This might be caused by the ICP phenomenon which has created a resistance for solute solution to flow within the porous substrates. According to Lim et al. [47], ICP is the major factor that leads to

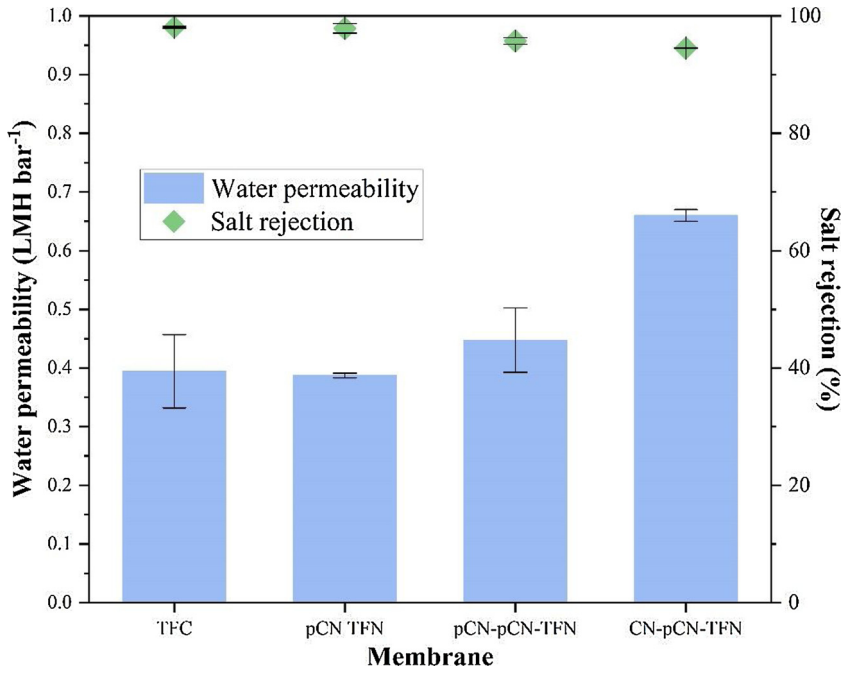

Fig. 6. Water permeability and salt rejection of TFC and TFN membranes (test condition: 15 bar, 25 °C, 2000 ppm NaCl solution).

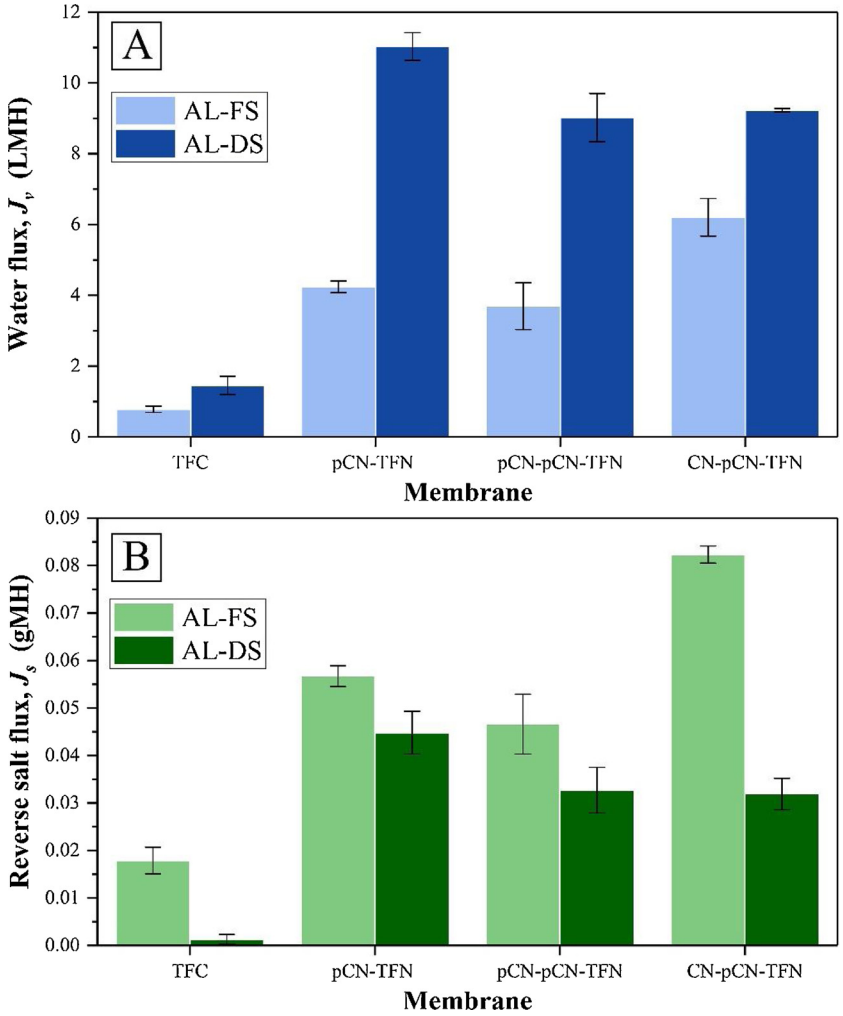

Fig. 7. FO performances on A) water flux and B) reverse solute flux on AL-FS mode and AL-DS mode.

Table 3
Comparison of FO and RO performances of TFC and TFN membranes.

Membrane	FO performance (AL-FS)	RO performance			
	Structural parameter, S value (mm)	Water permeability, A (L/m^2.h.bar)	Salt permeability, B($\times 10^{-8}$ m/s)	NaCl rejection, R(%)	Membrane skin properties, B/A (kPa)
TFC	27.4	0.395	2.910	98.08	26.54
pCN-TFN	2.96	0.387	1.97	97.89	18.28
pCN-pCN-TFN	3.74	0.448	7.68	95.74	61.74
CN-pCN-TFN	2.14	0.66	7.34	94.52	40.02

low water flux in FO. Embedding pCN within the substrate seems to be a promising strategy as it increased the hydrophilicity of the membrane and produced higher water flux compared to TFC. For pCN-TFN, the value of water flux in AL-FS mode increased to 4.24 LMH and it can be deduced that ICP has been mitigated [48]. The structural parameter calculated in Table 3 has further confirmed the suppression of ICP. The S parameter was reduced from 27.4 mm to 2.96 mm. Similarly, the performances of TFN with either CN or pCN embedded within the PA layer were also improved compared to TFC membrane. All the TFN showed higher water flux and lower reverse solute flux in AL-DS mode due to less severe ICP

One of the undesired effects of incorporating hydrophilic nanomaterial within the PA layer of TFN was the increase of water flux at the expenses of salt rejection due to the formation of voids at the polymer-filler interphase. Hence, in this study, one of the main purposes of incorporating pCN within the PSf substrate was to introduce positive charge on the substrate in order to improve the interaction between the PA layer and the substrate. With better interaction, denser layer of PA layer was formed on the substrate to ensure high salt rejection [49]. Simultaneously, the hydrophilic CN and pCN also created additional pathway to facilitate the transport of water molecule. This strategy allows the TFN membrane to exhibit high flux and rejection of NaCl solution.

In term of salt rejection, TFC and pCN-TFN exhibited salt rejection that was above 98%, which suggested that the PA layer was almost intact despite the incorporation of nanomaterials within the layer. On the other hand, slight decrease in the rejection was observed for pCN-pCN-TFN and CN-pCN-TFN. However, these TFN membrane still exhibited NaCl rejection that was comparable to that of commercial RO membrane. The surface charge that carried by pCN and CN has helped

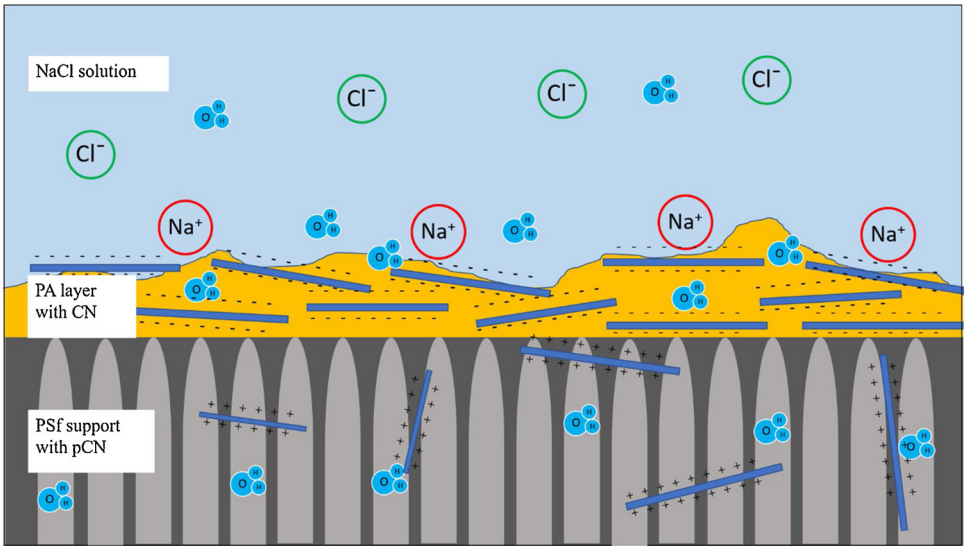

Fig. 8. Illustration on water pathway through the TFN membranes.

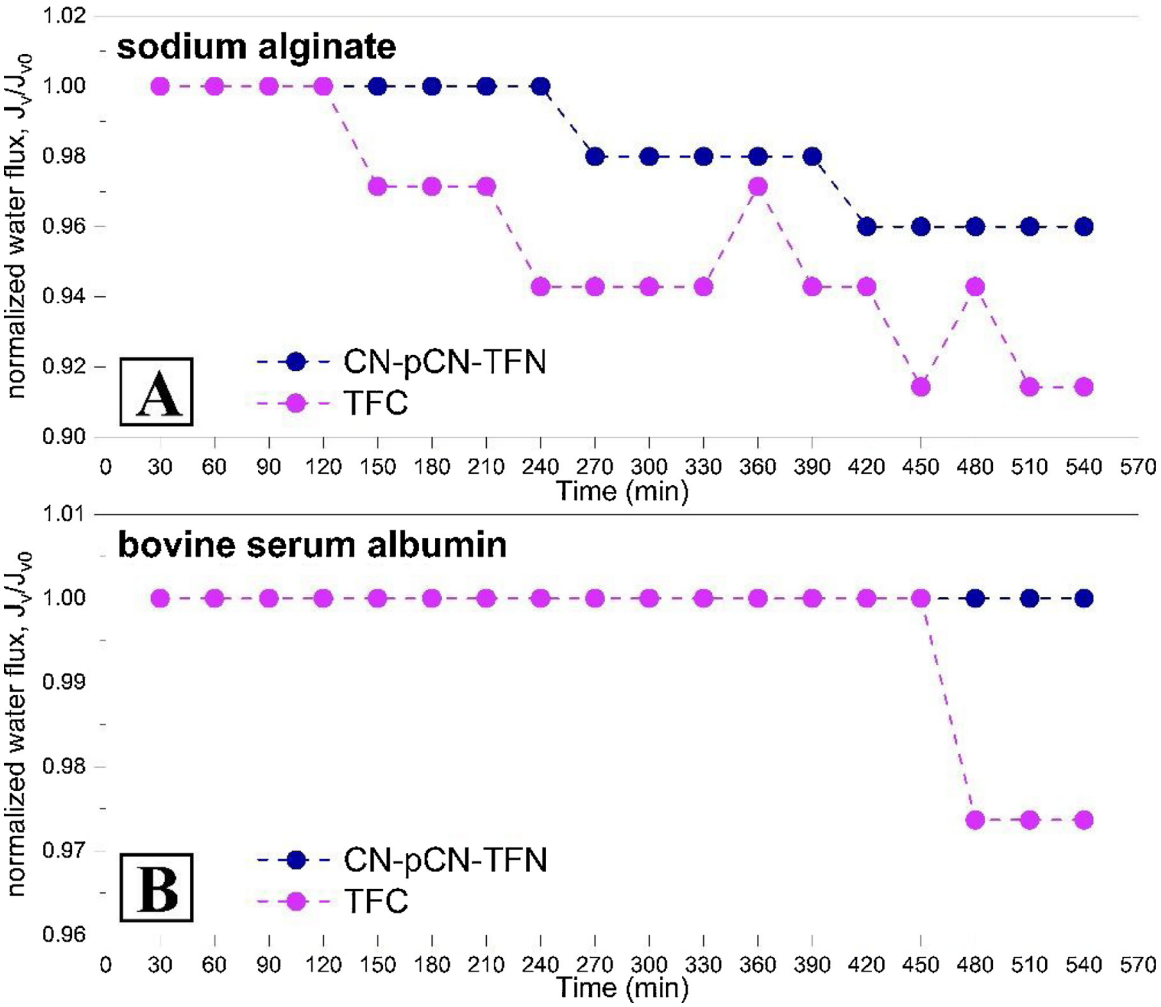

Fig. 9. Fouling behaviors of CN-pCN-TFN and TFC using (A) 500 ppm sodium alginate and (B) 500 ppm BSA as model foulants.

in rejecting the salt from permeating through. As illustrated in Fig. 8, Cl^- co-ions were repelled from the negatively charged surface whereas the Na^+ counterions were attracted to the surface and become more dominant at the water-membrane interface. However, the counterions could not firmly attach on the negatively charged surface due to Brownian motion effect. As a result, the accumulated Na^+ counterions has re-established the electroneutrality at the region sufficiently distant away from the membrane surface [50]. Consequently, both Na^+ and Cl^- ions can be effectively rejected by the charged surfaces.

Fig. 9 depicted the changes in water flux of CN-pCN-TFN and TFC in

Table 4
Comparison of FO and RO performances of mixed matrix membrane and TFN membrane.

Substrate		PA layer	NaCl rejection (%)	Pure water permeability ($Lm^{-2}h^{-1}b^{-1}$)	Reference
Polymer	Nanomaterial	Nanomaterial			
18% PES	1% PMAPS	–	TFC = 96.2 TFN = 95.8	TFC = 0.57 TFN = 0.69	[51]
15% PSf	0.33% INT	–	TFC = 58.0 TFN = 88.0	TFC = 0.27 TFN = 1.39	[15]
15% PSf	3% LDH	–	TFC = 83.8 TFN = 81.6	TFC = 1.96 TFN = 2.33	[52]
16% PSf	–	0.05 w/v% F-MWCNT	TFC = 70 TFN = 89.3	TFC = 3.1 TFN = 3.6	[53]
PS35	–	a-MWCNT-TNT	TFC = 97.8 TFN = 97.9	TFC = 0.47 TFN = 0.74	[4]
12% PES	–	100 ppm TW-OFs	TFC = 94.38 TFN = 93.96	–	[54]
14% PES	0.2% Fe_3O_4/ZnO	0.02% Fe_3O_4/ZnO	TFC = 96.3 TFN = 96.5	TFC = 1.96 TFN = 2.97	[55]
17.5% PSf	0.5% pCN	0.05% CN	TFC = 98 TFN = 94.5	TFC = 0.40 TFN = 0.67	This work

the presence of sodium alginate or BSA foulant. When sodium alginate was introduced as polysaccharide-based foulant at the feed, the water flux of TFC begun to decline after 2 h operation while CN-pCN-TFN was able to retain its original water flux two times longer than the former. After 9 h continuous operation, the water flux of TFC declined 8.6% whereas the water flux of CN-pCN-TFN only declined 4.0%. Similar trend was also observed when BSA was used as protein-based foulant. However, both TFC and CN-pCN-TFN were less susceptible to BSA fouling. The water flux of CN-pCN-TFN was unchanged throughout the 9 h testing period whereas TFC begun to be fouled by BSA after 7.5 h. These observations suggested that CN-pCN-TFN exhibited better anti-fouling property compared to TFC.

Table 4 tabulates the performance reported in the previous and current studies. Pan et al. [15] embedded imogolite nanotubes (INTs) in the PSf substrate to improve the hydrophilicity thus increase the water permeability from 1.96 LMHbar to 2.33 LMHbar. Although the improvement in salt rejection was observed, the salt rejection was still below 90%. Pardeshi et al. [52] incorporated layered double hydroxide nanoparticles (LDH) within the substrates to improve the water permeability. The water permeability increased but their NaCl rejection has been compromised. Other than that, M. Amini et al. [53] incorporated functionalized multiwalled carbon nanotube in the PA layer to have a better membrane performance. With only 0.05% of F-MWCNTs, their salt rejection and water permeability were improved significantly. In this work, embedding 0.5 wt% pCN in the PSf substrate has resulted in the increase in water flux without much compromising the salt rejection. Based on the comparisons, it is clear that there are still rooms of improvement for the membrane developed in this study. However, this work has explored the potential of CN to alter the properties of FO membrane for desalination. By tailoring the charges of the substrate and PA layer through the incorporation of CN and pCN with desired surface charges, the membrane performance can be improved.

4. Conclusions

In this study, the benefits of using pCN and CN in tailoring the surface properties of PA layer and intrinsic properties of substrate have been evidenced and discussed. Based on the performance of the membrane fabricated, TFC and pCN-TFN showed above 98% for salt rejection (NaCl) with water permeability of 0.4 LMH bar^{-1} and 0.39 LMH bar^{-1} respectively. When the pCN-pCN-TFN and CN-pCN-TFN were tested for water permeability and salt rejection, it showed a great performance for RO membranes. pCN-CN-TFN recorded about 0.45 LMH bar^{-1} with 95.7% salt rejection while CN-pCN-TFN improved the water permeability to 0.67 LMH bar^{-1} and 94.5% salt rejection. It is an ultimate target in membrane-based desalination to improve water productivity without significantly sacrificing the salt rejection. In term of performance in FO configuration, TFNs embedded with the hydrophilic nanomaterials exhibited enhanced water flux with better ICP resistance compared to TFC. Hence, the CN-pCN-TFN developed in this study holds potentials to be further optimized for improving the desalination performance.

All authors have participated in (a) conception and design, or analysis and interpretation of the data; (b) drafting the article or revising it critically for important intellectual content; and (c) approval of the final version.

Declaration of Competing Interest

Please check the following as appropriate:

All authors have participated in (a) conception and design, or analysis and interpretation of the data; (b) drafting the article or revising it critically for important intellectual content; and (c) approval of the final version.

This manuscript has not been submitted to, nor is under review at, another journal or other publishing venue.

The authors have no affiliation with any organization with a direct or indirect financial interest in the subject matter discussed in the manuscript

The following authors have affiliations with organizations with direct or indirect financial interest in the subject matter discussed in the manuscript:

Acknowledgements

The authors would like to acknowledge the financial supports provided by Ministry of Education Malaysia under HiCOE Grants (4J182), Fundamental Research grant Scheme (5F005) and Malaysia Research University Network Grant (4L862).

References

[1] D. Pimentel, M. Burgess, World Human Population Problems, Elsevier Inc., 2015, https://doi.org/10.1016/B978-0-12-409548-9.09303-9.
[2] U. Nations, Water for a Sustainable World, (2015).
[3] R. Jafarzadeh, J. Azamat, H. Erfan-niya, M. Hosseini, Applied Surface Science Molecular insights into effective water desalination through functionalized nanoporous boron nitride nanosheet membranes, Appl. Surf. Sci. 471 (2019) 921–928, https://doi.org/10.1016/j.apsusc.2018.12.069.
[4] I.W. Azelee, P.S. Goh, W.J. Lau, A.F. Ismail, K.C. Wong, M.N. Subramaniam, Enhanced desalination of polyamide thin film nanocomposite incorporated with acid treated multiwalled carbon nanotube-titania nanotube hybrid, Desalination 409 (2017) 163–170, https://doi.org/10.1016/j.desal.2017.01.029.
[5] M. Fathizadeh, H.N. Tien, K. Khivantsev, Z. Song, F. Zhou, Polyamide / nitrogen-

doped graphene oxide quantum dots (N-GOQD) thin film nanocomposite reverse osmosis membranes for high flux desalination, Desalination (2017) 1–8, https://doi.org/10.1016/j.desal.2017.07.014.
[6] N. Misdan, W.J. Lau, A.F. Ismail, Seawater Reverse Osmosis (SWRO) desalination by thin-film composite membrane — current development, challenges and future prospects, Desalination 287 (2012) 228–237, https://doi.org/10.1016/j.desal.2011.11.001.
[7] R.V. Linares, Z. Li, S. Sarp, S.S. Bucs, G. Amy, Science Direct Forward osmosis niches in seawater desalination and wastewater reuse, Water Res. 6 (2014), https://doi.org/10.1016/j.watres.2014.08.021.
[8] Y. Wang, R. Ou, Q. Ge, H. Wang, T. Xu, Preparation of polyethersulfone / carbon nanotube substrate for high-performance forward osmosis membrane, Desalination 330 (2013) 70–78, https://doi.org/10.1016/j.desal.2013.09.028.
[9] Q. Wang, X. Gao, Z. Ma, J. Wang, X. Wang, Y. Yang, C. Gao, Combined water flux enhancement of PES-based TFC membranes in ultrasonic-assisted forward osmosis processes, J. Ind. Eng. Chem. 64 (2018) 266–275, https://doi.org/10.1016/j.jiec.2018.03.024.
[10] M. Ghanbari, D. Emadzadeh, W.J. Lau, H. Riazi, D. Almasi, A.F. Ismail, Minimizing structural parameter of thin film composite forward osmosis membranes using polysulfone / halloysite nanotubes as membrane substrates, Desalination 377 (2016) 152–162, https://doi.org/10.1016/j.desal.2015.09.019.
[11] T.A. Otitoju, R.A. Saari, A.L. Ahmad, Progress in the modification of reverse osmosis (RO) membranes for enhanced performance, J. Ind. Eng. Chem. 67 (2018) 52–71, https://doi.org/10.1016/j.jiec.2018.07.010.
[12] B. Jeong, E.M.V. Hoek, Y. Yan, A. Subramani, X. Huang, G. Hurwitz, A.K. Ghosh, A. Jawor, Interfacial polymerization of thin film nanocomposites: A new concept for reverse osmosis membranes, J. Memb. Sci. 294 (2007) 1–7, https://doi.org/10.1016/j.memsci.2007.02.025.
[13] P.S. Goh, A.F. Ismail, A review on inorganic membranes for desalination and wastewater treatment, Desalination (2017), https://doi.org/10.1016/j.desal.2017.07.023 0–1..
[14] D. Emadzadeh, W.J. Lau, A.F. Ismail, Synthesis of thin film nanocomposite forward osmosis membrane with enhancement in water flux without sacrificing salt rejection, Desalination 330 (2013) 90–99, https://doi.org/10.1016/j.desal.2013.10.003.
[15] Y. Pan, Q. Zhao, L. Gu, Q. Wu, Thin film nanocomposite membranes based on imologite nanotubes blended substrates for forward osmosis desalination, Desalination (2017), https://doi.org/10.1016/j.desal.2017.04.019 0–1.
[16] D. Emadzadeh, W.J. Lau, M. Rahbari-sisakht, A. Daneshfar, M. Ghanbari, A. Mayahi, A novel thin film nanocomposite reverse osmosis membrane with superior anti-organic fouling affinity for water desalination, Desalination 368 (2015) 106–113, https://doi.org/10.1016/j.desal.2014.11.019.
[17] J. Zhao, Y. Liu, Y. Wang, H. Li, J. Wang, Z. Li, Boron doped graphitic carbon nitride dots dispersed on graphitic carbon nitride/graphene hybrid nanosheets as high performance photocatalysts for hydrogen evolution reaction, Appl. Surf. Sci. 470 (2019) 923–932, https://doi.org/10.1016/j.apsusc.2018.11.138.
[18] P. Niu, L. Zhang, G. Liu, H. Cheng, Graphene-like carbon nitride nanosheets for improved photocatalytic activities, Adv. Funct. Mater. (2012) 4763–4770, https://doi.org/10.1002/adfm.201200922.
[19] M. Sihor, P. Praus, L. Svoboda, M. Ritz, I. Troppov, K. Ko, Graphitic carbon nitride: synthesis, characterization and photocatalytic decomposition of nitrous oxide, Mater. Chem. Phys. 193 (2017) 438–446, https://doi.org/10.1016/j.matchemphys.2017.03.008.
[20] J. Li, B. Shen, Z. Hong, B. Lin, B. Gao, Y. Chen, A facile approach to synthesize novel oxygen-doped g-C3N4 with superior visible-light photoreactivity, Chem. Commun. 4 (2012) 12017–12019, https://doi.org/10.1039/c2cc35862j.
[21] Y. Wang, R. Ou, H. Wang, T. Xu, Graphene oxide modified graphitic carbon nitride as a modifier for thin film composite forward osmosis membrane, J. Memb. Sci. 475 (2015) 281–289, https://doi.org/10.1016/j.memsci.2014.10.028.
[22] J. Yin, B. Deng, Polymer-matrix nanocomposite membranes for water treatment, J. Memb. Sci. 479 (2015) 256–275, https://doi.org/10.1016/j.memsci.2014.11.019.
[23] J. Zhu, P. Xiao, H. Li, A.C. Carabineiro, Graphitic Carbon Nitride: Synthesis, Properties, And Applications In Catalysis, ACS Publications, 2014.
[24] Z. Zhou, J.Y. Lee, T. Chung, A.L. Ds, A.L. Fs, Thin film composite forward-osmosis membranes with enhanced internal osmotic pressure for internal concentration polarization reduction, Chem. Eng. J. 249 (2014) 236–245, https://doi.org/10.1016/j.cej.2014.03.049.
[25] B.W. Ninham, On progress in forces since the DLVO theory, Adv. Colloid Interface Sci. 83 (1999) 1–17, https://doi.org/10.1016/S0001-8686(99)00008-1.
[26] I.A. Mudunkotuwa, V.H. Grassian, Citric Acid Adsorption on TiO2 Nanoparticles in Aqueous Suspensions at Acidic and Circumneutral pH: Surface Coverage, Surface Speciation, and Its Impact on Nanoparticle - Nanoparticle Interactions, (2010), pp. 14986–14994.
[27] C. Huang, W. Zhang, Z. Yan, J. Gao, W. Liu, P. Tong, L. Zhang, Protonated mesoporous graphitic carbon nitride for rapid and highly efficient removal of microcystins, RSC Adv. 5 (2015) 45368–45375, https://doi.org/10.1039/C5RA01415H.
[28] J. Wang, D. Hao, J. Ye, N. Umezawa, Determination of crystal structure of graphitic carbon nitride: ab initio evolutionary search and experimental validation, ACS Publications (2017), https://doi.org/10.1021/acs.chemmater.6b02969.
[29] T. Tyborski, C. Merschjann, S. Orthmann, F. Yang, Crystal Structure Of Polymeric Carbon Nitride And The Determination Of Its, 395402 (n.d.) (2019), https://doi.org/10.1088/0953-8984/25/39/395402.
[30] M. Aleksandrzak, W. Kukulka, E. Mijowska, Applied Surface Science Graphitic carbon nitride / graphene oxide / reduced graphene oxide nanocomposites for photoluminescence and photocatalysis, Appl. Surf. Sci. 398 (2017) 56–62, https://doi.org/10.1016/j.apsusc.2016.12.023.
[31] A.P. Qiu, C. Xu, H. Chen, One step synthesis of oxygen doped porous graphitic carbon nitride with remarkable improvement of photo-oxidation activity: role of oxygen on visible light photocatalytic activity, Applied Catal. B, Environ. (2017), https://doi.org/10.1016/j.apcatb.2017.01.058.
[32] C. Huang, W. Zhang, Z. Yan, J. Gao, W. Liu, P. Tong, L. Zhang, Protonated mesoporous graphitic carbon nitride for rapid and highly efficient removal of microcystins, RSC Adv. 5 (2015) 45368–45375, https://doi.org/10.1039/C5RA01415H.
[33] R. Schlo, A. Thomas, A. Fischer, F. Goettmann, M. Antonietti, J. Mu, J.M. Carlsson, Graphitic Carbon Nitride Materials : Variation of Structure and Morphology and Their Use As Metal-free Catalysts, (2008), pp. 4893–4908, https://doi.org/10.1039/b800274f.
[34] W. Ong, L. Tan, S. Chai, S. Yong, A. Rahman, Surface charge modi fi cation via protonation of graphitic carbon nitride (g-C 3 N 4) for electrostatic self-assembly construction of 2D / 2D reduced graphene oxide (rGO)/ g-C 3 N 4 nanostructures toward enhanced photocatalytic reduction of carbon dio, Nano Energy 13 (2015) 757–770, https://doi.org/10.1016/j.nanoen.2015.03.014.
[35] X. Zhang, J. Tian, Z. Ren, W. Shi, Z. Zhang, High performance thin-film composite (TFC) forward osmosis (FO) membrane fabricated on novel hydrophilic disulfonated poly (arylene ether sulfone) multiblock copolymer / polysulfone substrate, J. Memb. Sci. 520 (2016) 529–539, https://doi.org/10.1016/j.memsci.2016.08.005.
[36] T. Sirinupong, W. Youravong, D. Tirawat, W.J. Lau, G.S. Lai, A.F. Ismail, Synthesis and characterization of thin film composite membranes made of PSF-TiO 2 / GO nanocomposite substrate for forward osmosis applications, Arab. J. Chem. (2017), https://doi.org/10.1016/j.arabjc.2017.05.006.
[37] S. Al, A. Haroutounian, C.J. Wright, N. Hilal, Thin Film Nanocomposite (TFN) membranes modified with polydopamine coated metals / carbon-nanostructures for desalination applications, Desalination 427 (2018) 60–74, https://doi.org/10.1016/j.desal.2017.10.011.
[38] M. Fathizadeh, A. Aroujalian, A. Raisi, Effect of added NaX nano-zeolite into polyamide as a top thin layer of membrane on water flux and salt rejection in a reverse osmosis process, J. Memb. Sci. 375 (2011) 88–95, https://doi.org/10.1016/j.memsci.2011.03.017.
[39] B. Khorshidi, T. Thundat, D. Pernitsky, M. Sadrzadeh, Permeation properties of thin film composite polyamide membrane, J. Memb. Sci. 535 (2017) 248–257, https://doi.org/10.1016/j.memsci.2017.04.052.
[40] G.S. Lai, W.J. Lau, P.S. Goh, A.F. Ismail, N. Yusof, Y.H. Tan, Graphene oxide incorporated thin film nanocomposite nanofiltration membrane for enhanced salt removal performance, Desalination 387 (2016) 14–24, https://doi.org/10.1016/j.desal.2016.03.007.
[41] W.J. Lau, A.F. Ismail, P.S. Goh, N. Hilal, B.S. Ooi, A.F. Ismail, P.S. Goh, N. Hilal, B.S.O. Characterization, W.J. Lau, A.F. Ismail, P.S. Goh, N. Hilal, B.S. Ooi, Characterization methods of thin film composite nanofiltration membranes characterization methods of thin film composite nanofiltration membranes, Sep. Purif. Rev. 2119 (2015), https://doi.org/10.1080/15422119.2014.882355.
[42] N. Misdan, W.J. Lau, A.F. Ismail, T. Matsuura, Formation of thin film composite nanofiltration membrane: effect of polysulfone substrate characteristics, Desalination 329 (2013) 9–18.
[43] G. Hurwitz, G.R. Guillen, E.M.V. Hoek, Probing polyamide membrane surface charge, zeta potential, wettability, and hydrophilicity with contact angle measurements, J. Memb. Sci. 349 (2010) 349–357, https://doi.org/10.1016/j.memsci.2009.11.063.
[44] A. Ghaee, M.M. Zerafat, P. Askari, S. Sabbaghi, B. Sadatnia, Fabrication of polyamide thin-film nanocomposite membranes with enhanced surface charge for nitrate ion removal from water resources, Environ. Technol. 0 (2016) 1–10, https://doi.org/10.1080/09593330.2016.1231223.
[45] V.T. Do, C.Y. Tang, M. Reinhard, J.O. Leckie, Degradation of polyamide nanofiltration and reverse osmosis membranes by hypochlorite, Environ Sci Technol. (2012).
[46] M.R. Teixeira, M.J. Rosa, M. Nyström, The role of membrane charge on nanofiltration performance, J. Memb. Sci. 265 (2005) 160–166, https://doi.org/10.1016/j.memsci.2005.04.046.
[47] S. Lim, M. Jun, S. Phuntsho, L.D. Tijing, G.M. Nisola, W. Shim, W. Chung, H. Kyong, Dual-layered nanocomposite substrate membrane based on polysulfone / graphene oxide for mitigating internal concentration polarization in forward osmosis, Polymer (Guildf). 110 (2017) 36–48, https://doi.org/10.1016/j.polymer.2016.12.066.
[48] P. Dou, S. Zhao, J. Song, H. He, Q. She, X.M. Li, Y. Zhang, T. He, Forward osmosis concentration of a vanadium leaching solution, J. Memb. Sci. 582 (2019) 164–171, https://doi.org/10.1016/j.memsci.2019.04.012.
[49] R. Han, Z. Xiao, Effect of LSCF content on the performance of LSCF / PES mixed matrix membranes, Desalination 359 (2015) 108–112, https://doi.org/10.1016/j.desal.2014.12.015.
[50] H.F. Ridgway, J. Orbell, S. Gray, Molecular simulations of polyamide membrane materials used in desalination and water reuse applications : recent developments and future prospects, J. Memb. Sci. 524 (2017) 436–448, https://doi.org/10.1016/j.memsci.2016.11.061.
[51] S. Sahebi, S. Phuntsho, Y.C. Woo, M.J. Park, L.D. Tijing, S. Hong, H.K. Shon, Effect of sulphonated polyethersulfone substrate for thin film composite forward osmosis membrane, Desalination. 389 (2016) 129–136, https://doi.org/10.1016/j.desal.2015.11.028.
[52] P.M. Pardeshi, A.K. Mungray, A.A. Mungray, Polyvinyl chloride and layered double hydroxide composite as a novel substrate material for the forward osmosis membrane, Desalination (2017) 1–11, https://doi.org/10.1016/j.desal.2017.01.041.
[53] R. Ramezani Darabi, M. Jahanshahi, M. Peyravi, A support assisted by photocatalytic Fe3O4/ZnO nanocomposite for thin-film forward osmosis membrane, Chem. Eng. Res. Des. 133 (2018) 11–25, https://doi.org/10.1016/j.cherd.2018.02.029.